Tunable Multiple Fano Resonances and Stable Plasmonic Band-Stop Filter Based on a Metal-Insulator-Metal Waveguide

Chen Zhou[1] · Yiping Huo[1] · Yiyuan Guo[1] · Qiqiang Niu[1]

Abstract

A metal-insulator-metal (MIM) waveguide consisting of two stub resonators and a ring resonator is proposed, which can be used as refractive index sensor and stop-band filter at the same time. The transmission characteristics of the MIM waveguide structure is studied by the finite element method (FEM). The simulation results show that the typical Fano profile and multiple Fano resonances can be achieved. According to the analysis, the range of stop-band and the multiple Fano resonance positions can be adjusted flexibly and independently by adjusting the aggregate parameters of the MIM waveguide structure. Moreover, it is also found that the two Fano resonances at both ends of the stop band can be determined by the two stubs, and the other two Fano resonances are regulated by the ring resonator. In addition, the spectral position of multi-Fano resonances is highly sensitive to the radius of the ring resonator and the refractive index of the filled medium. The maximum sensitivity and the figure of merit (FOM) of the MIM waveguide structure are 1650 nm/RIU and 117.8 in magnitude, respectively. These results provide a reference for implementing high-sensitivity sensors and large-bandwidth stop-band filter in MIM waveguide coupling systems based on multi-Fano resonance effect.

Keywords Surface plasmon · Fano resonance · The refractive index sensitivity · The band-stop filter · The figure of merit (FOM)

Introduction

Surface plasmon polaritons (SPPs) are the electromagnetic waves, which can be generated by the interaction between incident light and metal structure [1, 2]. The amplitude of SPP optical field decays exponentially in the direction perpendicular to the metal-insulator interface [3, 4]; therefore, SPPs only exist on the interface between metal and dielectric. Because the SPPs has the excellent characteristics of breaking the diffraction limit [5, 6], it has very important applications in nanolevel optical manipulation, transmission, processing, and control in high-density photonic integrated circuits [7–10]. In recent years, the various devices based on SPPs, such as the metal-insulator-metal (MIM) waveguide structures, have received more attention and have been extensive researched because of their strong local area capability and acceptable propagation length [11–13].

At present, people have conducted extensive research on Fano resonance [14, 15] and electromagnetic induced transparency (EIT) [16, 17] effect based on the interaction between incident light and metal nanostructure. Fano resonance initially originated from the interference between continuous state and discrete state in the ionization process of condensed matter physics, and its resonance line shape has an obvious asymmetry type [13]. Fano resonance shows good sensitivity to the changes of structural parameter and environmental refractive index, and has important applications in biosensing, lasers, and optical modulators [18, 19]. Several sensors based on MIM waveguide structure have been studied and reported now, which indicate that Fano resonance–based refractive index sensors can be implemented in MIM waveguide structure [20–22].

In this paper, a MIM waveguide structure is designed, which is coupled with two stub resonators and a ring resonator. By the numerical simulation based on the finite element method, the transmission spectrum and magnetic field distribution are analyzed. Changing the structure parameters of the MIM waveguide and the refractive index of the filling medium of the ring resonator cavity, the simulation results

✉ Yiping Huo
yphuo@snnu.edu.cn

1 School of Physics and Information Technology, Shaanxi Normal University, 710119 Xi'an, P.R. China

show that the functions of refractive index sensor and band-stop filter based on multi-Fano resonance can be realized simultaneously.

Model and Calculation Method

Figure 1 shows a two-dimensional (2D) schematic diagram of a coupled system consisting of a MIM waveguide with two stub resonators and a ring resonator. When the depth of the z-direction is deep enough, the simulation results of the three-dimensional model are the same as that of the two-dimensional model and the calculation complexity is greatly reduced; therefore, the two-dimensional model is used in the whole calculation [23].

In Fig. 1, the blue part represents silver and the white part represents air ($n = 1.0$). The width of the bus waveguide is W. As can be seen from Fig. 1 of reference [24], the SPPs can be excited by the input light, which is the transverse magnetic (TM) field mode obtained from boundary mode analysis. The coupling distance between the bus waveguide and the ring cavity is g. The lengths of the two stubs are expressed as H_1 and H_2, and their widths are W_1 and W_2, respectively. The distance between the left stub and the ring resonator is L_1, the distance between the right stub and the ring resonator is L_2, and L_1 is not equal to L_2. The inner radius and outer radius of the ring resonator are denoted by r and R, respectively. Initially, the filled medium is air and its refractive index is $n = 1.0$.

In the calculation process, the relative dielectric constant of the silver material we chose can be defined by the Debye-Ruder dispersion model [25, 26]:

$$\varepsilon(\omega) = \varepsilon_\infty - \frac{\omega_p^2}{\omega(\omega + i\gamma)} \tag{1}$$

In Eq. 1, the plasma frequency of silver is $\omega_p = 1.37 \times 10^{16}$ s^{-1}, the damping constant is $\gamma = 2.73 \times 10^{13}$ s^{-1}, and the dielectric constant of the infinite frequency is $\varepsilon_\infty = 3.7$.

For the proposed waveguide coupled system, the sensing performance is studied by analyzing the resonance wavelength shifts. The resonant wavelength and the real part of the MIM waveguide structure's effective refractive index based on the standing wave theory [27] can be represented as Eqs. (2) and (3), respectively.

$$\lambda_m = \frac{2\mathrm{Re}(n_{\mathrm{eff}})L}{m - \psi/\pi} m = 1, 2, 3 \cdots \tag{2}$$

$$\mathrm{Re}(n_{\mathrm{eff}}) = \left[\varepsilon_m + (k/k_0)^2\right]^{1/2} \tag{3}$$

where L represents the effective length of the cavity, ψ represents the phase shift caused by the reflection of SPPs at the interface of the metal and insulator, and the positive integer m represents the number of antinodes of the standing wave SPPs.

To illustrate the Fano resonance phenomenon by the temporal coupled mode theory [28] in detail, the amplitudes of the SPP wave of the structure are denoted by Si± ($i = 1, 2$). The subscripts denote the input and output electromagnetic wave of the cavity (as shown in Fig. 1), respectively. The coupling coefficients between the input bus waveguide and the first stub, between the bus waveguide and the ring cavity, and between the output bus waveguide and the second stub are κ_1, κ_2, and κ_3, respectively. When an optical wave with a certain frequency is launched only from the input port of the MIM waveguide ($S_{2+} = 0$), the time evolution amplitude of the stubs A_S and the time evolution amplitude of the ring cavity A_R can be derived as

$$\frac{\partial A_s}{\partial t} = (j\omega_s - \kappa_1 - \kappa_2 - \kappa_3)A_s + \kappa_1 S_1 + \kappa_2 S_2 + \kappa_3 A_R \tag{4}$$

Fig. 1 Two-dimensional schematic diagram of the MIM waveguide system
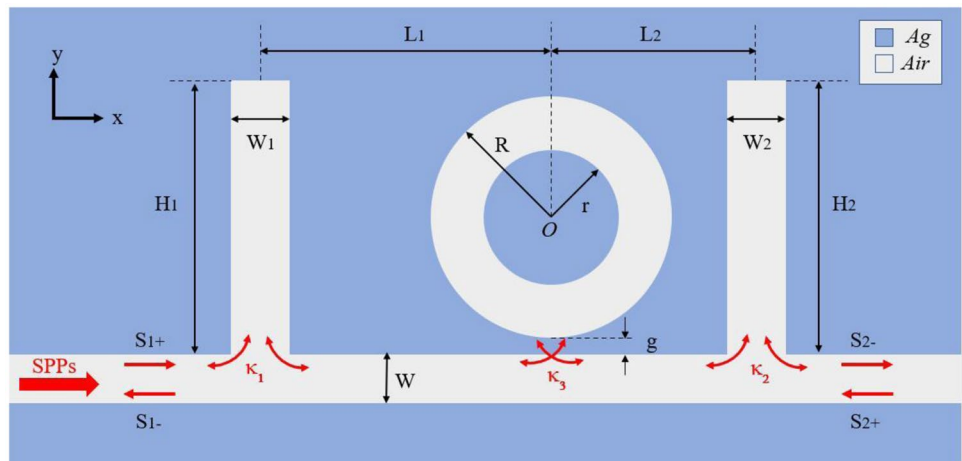
$$\frac{\partial A_{\mathrm{R}}}{\partial t} = (j\omega_{\mathrm{R}} - \kappa_3)A_{\mathrm{R}} + \kappa_3 A_S \tag{5}$$

where j is the imaginary unit ($j^2 = -1$) and ω_s and ω_{R} are the resonance frequencies of the stubs and the ring cavities, respectively. Eqs. 6 and 5

In accordance with the energy conservation law, the amplitude of the input and output optical waves in the coupled waveguides are derived by Eq. 6

$$S_{2-} = S_{1+} + \sqrt[2]{K_2}A_\mathrm{s} \tag{6}$$

The transmittance **T** can be obtained as follows: Eq. 7

$$T = \left|\frac{s_{2-}}{s_{1+}}\right|^2 = \left|\frac{\kappa_1\kappa_2\left[j(\omega - \omega_R) + \kappa_3^2\right]}{\left[j(\omega - \omega_S) + \kappa_1^2 + \kappa_2^2 + \kappa_3^2\right]\left[j(\omega - \omega_R) + \kappa_3^2\right] - \kappa_3^2}\right|^2 \tag{7}$$

In the following section, the propagation characteristics of the coupling structure are simulated by COMSOL Multiphysics software. During the simulation, the absorbing boundary of the bottom and top of the coupled structure is set as the same PML condition.

Results and Discussion

Transmission Properties of the MIM Waveguide System

In order to investigate the transmission spectrum properties of this MIM waveguide system, it must simulate the MIM waveguide structure under varying parameters. The initial values of the MIM waveguide structural parameters are $W = 50$ nm, $W_1 = W_2 = 100$ nm, $L_1 = 560$ nm, $L_2 = 500$ nm, $R = 300$ nm, $r = 160$ nm, $H_1 = H_2 = 720$ nm, and $g = 20$ nm.

Firstly, the transmission properties of the MIM structure are examined, and the results are shown in Fig. 2. It is clear that four Fano resonances with asymmetric lines can be obtained in the transmission spectrum of the MIM structure. These four Fano resonances are labeled as F1, F2, F3, and F4, and their resonance peak positions are $\lambda 1 = 829$ nm, $\lambda 2 = 1039$ nm, $\lambda 3 = 1312$ nm, and $\lambda 4 = 1625$ nm, respectively. The reflection losses of the four resonance positions are −27.1 dB, −21.5 dB, −20.2 dB, and −28.3 dB, respectively, and they are all less than −20 dB, which shows that our simulation process is appropriate. In addition, it can be found that a U shape appears in the transmission spectrum from 1039 to 1312 nm, so the designed structure achieves band-stop filtering function. Interestingly, this U-shaped transmission spectrum is composed of two opposite Fano lines, which are F2 and F3. The band-stop width is defined as the range of wavelengths with transmittance less than 1%. Therefore,
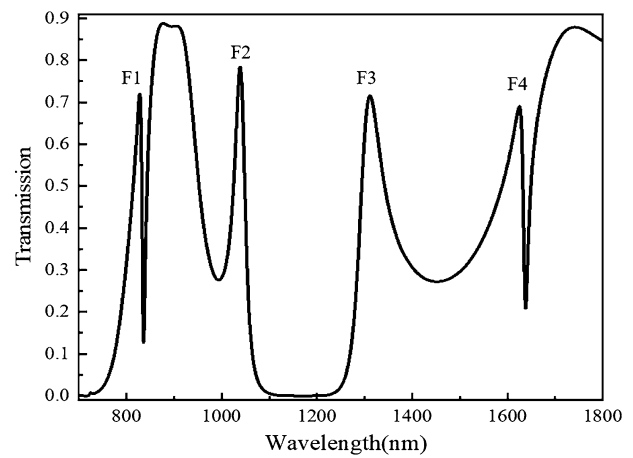

Fig. 2 Transmission characteristics of the MIM waveguide structure

the stop band formed by the U-shaped transmission spectrum begins at $\lambda 5 = 1092$ nm and ends at $\lambda 6 = 1241$ nm, respectively, so the stop band width is $\Delta = 149$ nm.

In order to better understand the specific resonance conditions of different Fano resonance, Fig. 3a–d show the magnetic field distributions of F1, F2, F3, and F4, respectively. Figure 3e, f are the magnetic field distributions at $\lambda 5 = 1092$ nm and $\lambda 6 = 1241$ nm. Firstly, we can easily find that both stubs in the MIM waveguide structure participate in the four Fano resonances. However, on the one hand, it can be found that the ring resonator participates in the resonance F1 and F4 as shown in Fig. 3a, d. On the other hand, the ring resonator does not participate in the resonance F2 and F3 as shown in Fig. 3b, c, those two resonance results are only caused by the two stubs. The ring resonator can be used to regulate the two resonances, F1 and F4. Secondly, as shown in Fig. 3e, f, the SPPs are blocked by the second stub, and normal transmission cannot be continued at $\lambda 5 = 1092$ nm, while the SPPs can transmit normally at $\lambda 6 = 1241$ nm. The two Fano resonances F2 and F3 on the U-shaped line both result from the coupling of the strong trapped resonance in the FP resonator and weak resonance in the tooth cavity. Therefore, the positions of the peaks can be controlled by the space between the teeth-shaped cavities, which means that the band-stop width of the U-shaped transmission spectrum can be regulated finely.

It can be found that the MIM waveguide structure proposed in this paper, which provides a way to realize multiple Fano resonances and a large band device with a certain band-stop filtering function. In order to understand the mechanism of Fano resonances and optimize the performance the band-stop filter, the transmission spectra of the MIM waveguide structure under different conditions are simulated.
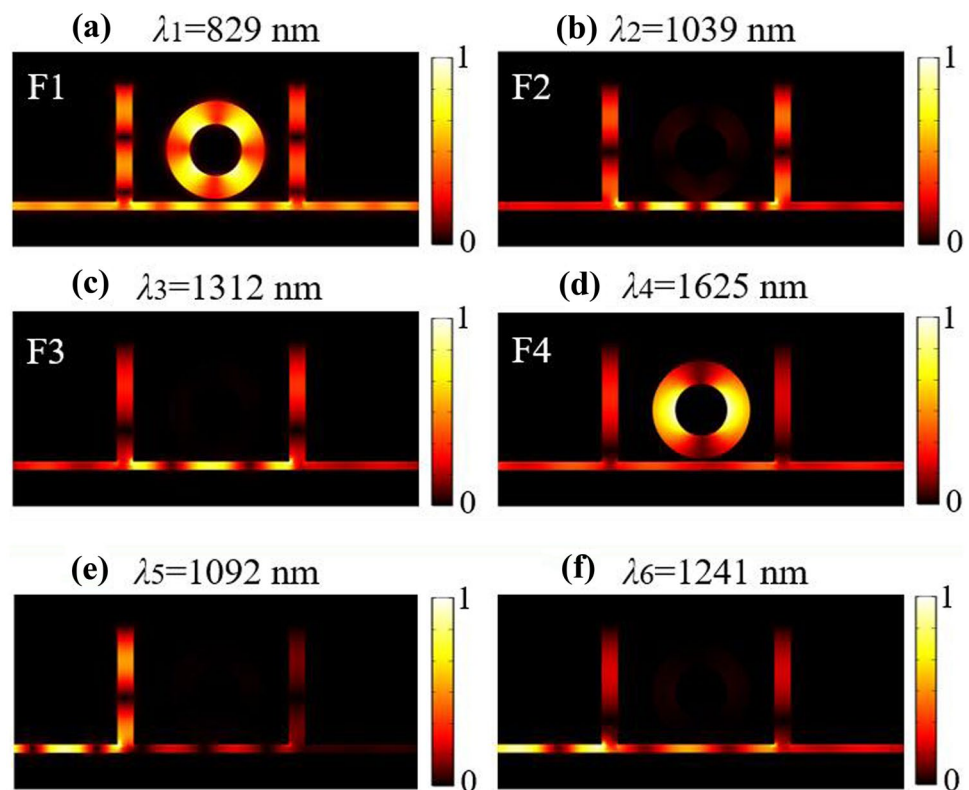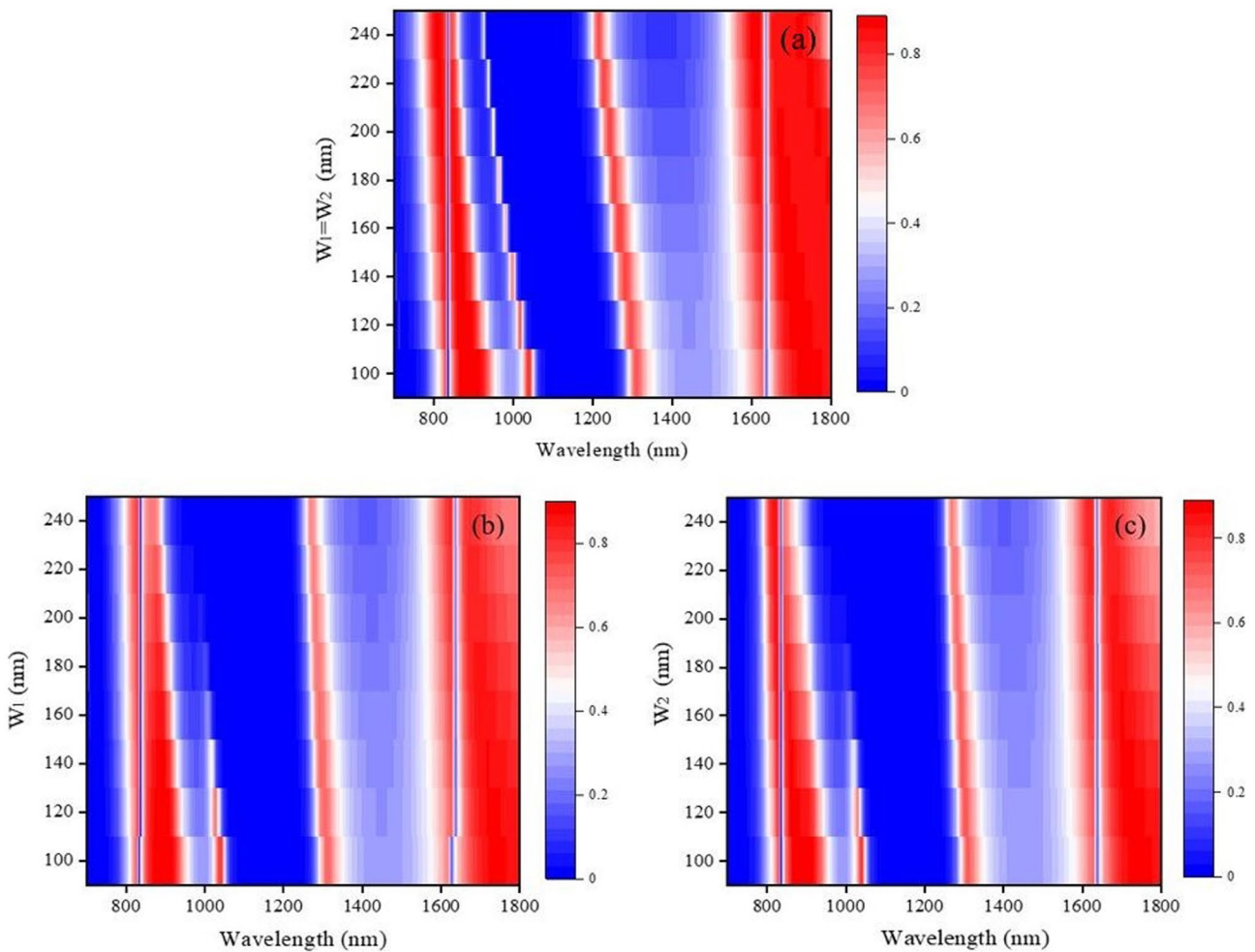
Influence of Parameters W_1 and W_2 on the Transmission Spectrum of the MIM Waveguide

As shown in Fig. 4, the effect of the width of two stubs on the transmittance of the MIM waveguide was studied. As shown in Fig. 4a, for F1 and F4 resonance, it can be seen that the resonance positions and resonance intensities have not changed when W_1 and W_2 increase at the same time. This behavior is also similar to independent increase of W1 or W2, as Fig. 4b, c show. The resonance positions and resonance intensities of F1 and F4 are not adjusted by the stubs because they are determined by the ring resonator. When W_1 and W_2 increase at the same time or increase alone, F2 resonance blue shifts significantly, and its intensity decreases. However, the decrease of F2 resonance intensity when W1 and W2 increase together is significantly less than the decrease when W1 or W2 increased alone. For F3 resonance, when W_1 and W_2 increase at the same time, it will undergo a significant blue shift. However, when W_1 or W_2 is increased alone, the position of F3 resonance will have a very weak blue shift, which can be regarded as unchanged basically. For the width of the stop band, when W_1 and W_2 increase at the same time, the blue shift degrees of F2 and F3 are similar, so the width of the stop band also blue shifts significantly while the stop width of the band remain unchanged. But

when W_1 or W_2 increases alone, especially when W_1 or W_2 is greater than 200 nm, although the resonance valley of F3 remains unchanged, the F2 resonance mode basically disappears, which directly leads to the width of the stop band increases rapidly. It can be seen that increasing the widths of the two stubs W_1 and W_2 at the same time can change the band range of the band-stop filter, increasing the width of the two stubs W_1 and W_2 alone can expand the stopband bandwidth of the band-stop filter.

Influence of Parameters L_1 and L_2 on the Transmission Spectrum of the MIM Waveguide Structure

As shown in Fig. 5a, b, the influence of changing the horizontal distance L_1 and L_2 between the two stubs and the center of the ring on the transmittance of the MIM waveguide is studied. When L_1 and L_2 increase, respectively, the resonance positions and resonance intensities of F1 and F4 remain unchanged, because F1 and F4 are determined by the ring resonator and are not adjusted by the stubs. Both F2 and F3 resonances have a significant red shift with the increase of L_1 or L_2. However, when L_1 is greater than 760 nm or L_2 is greater than 700 nm, F2 resonance disappears basically. So, changing the value of L1 or L2 is another effective method to expand the stopband bandwidth of the band-stop filter.

Fig. 4 Influence of parameters W_1 and W_2 on the transmission spectrum of the MIM waveguide, when (**a**) W_1 and W_2 are changed, (**b**) only W_1 is changed, and (**c**) only W_2 is changed
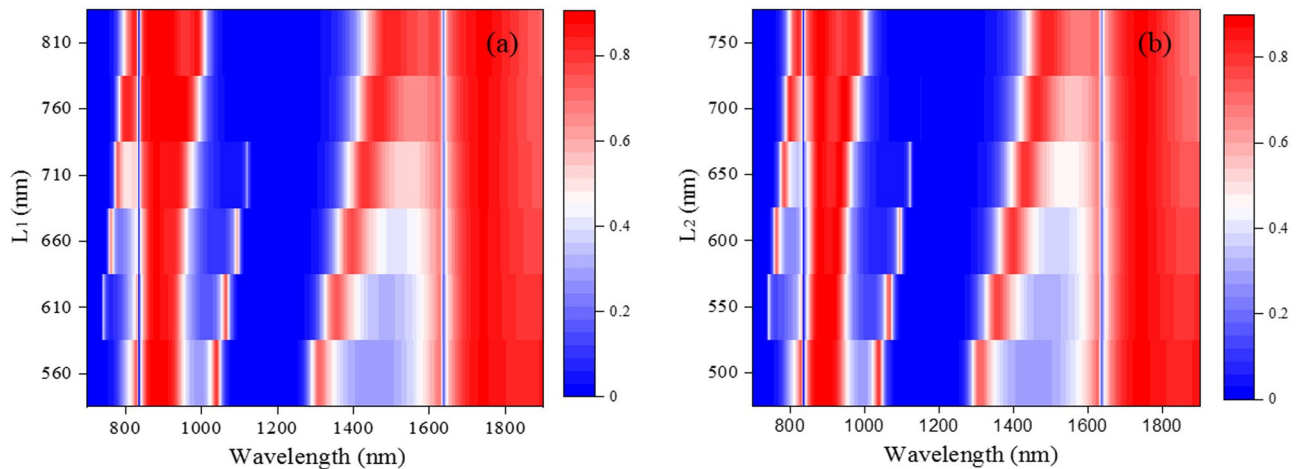
Influence of Parameters *r* and *g* on the Transmission Spectrum of the MIM Waveguide Structure

As shown in Fig. 6a, the change in the radius of the ring resonator *r* also has a significant effect on the transmittance of the MIM waveguide. As the inner radius *r* of the ring resonator increases from 140 to 180 nm, the resonance intensity of F1 and F4 increases rapidly and a significant redshift occurs, and the redshift degree of F4 is significantly greater than that of F1, indicating that F4 is more sensitive to the change of the inner ring. At the same time, it can also be found that the resonance position and resonance intensity of F2 and F3 remain unchanged, which also verifies the conclusion that changing the parameters of the ring will not affect F2 and F3 resonance. Therefore, the U-shaped transmission spectrum determined by F2

and F3 and the stopband filter with a stopband width of $\Delta = 149$ nm have strong stability characteristics.

When the distance between the ring resonator and the waveguide *g* is changed, the transmittance of the MIM waveguide is also affected, as shown in Fig. 6b. At this situation, it can be found that when the value of *g* increases from 10 to 50 nm, the resonance positions of F1 and F4 are almost unchanged, and the modulation depth of F1 and F4 decreases, so the resonance intensity decreases. From Fig. 6b, it can be seen that as *g* further increases to 60 nm, the F1 and F4 resonances will disappear, and the ring resonator will no longer participate in the coupling. In this case, the transmission characteristic of the waveguide structure is the same as the transmission characteristic without the ring resonator, as shown by the dotted curve in Fig. 6b.

Fig. 5 Influence of parameters: (**a**) L_1 and (**b**) L_2 on the transmission characteristics of the MIM waveguide
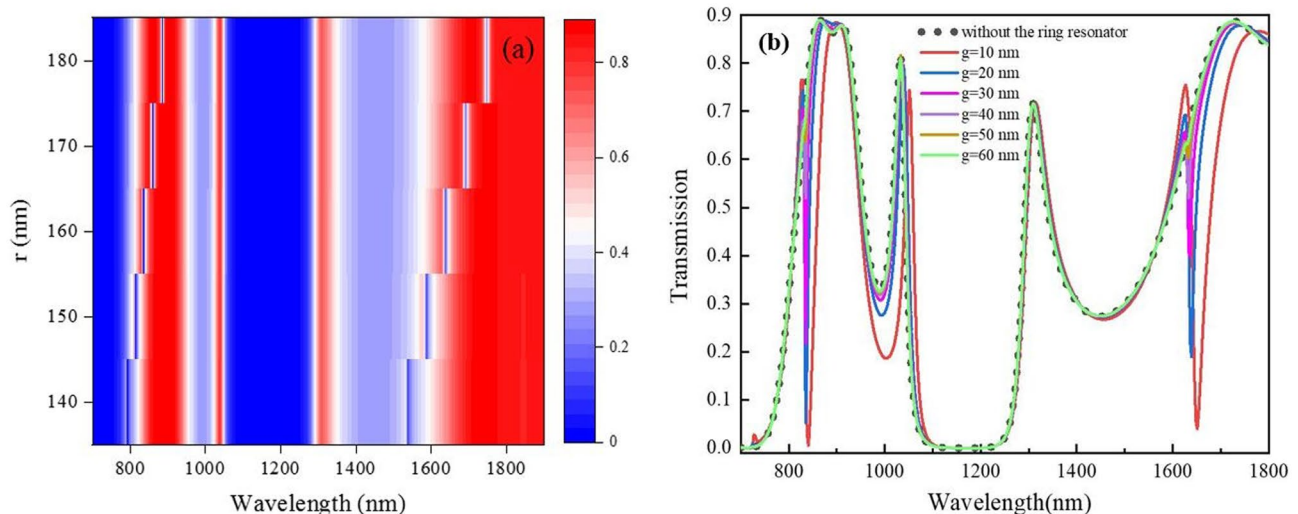
Influence of Refractive Index Environments on the Transmission of the MIM Waveguide Structure

In recent years, the MIM structure have been intensively studied as refractive index–sensitive sensors in the biological and chemical fields, such as the solution concentration and pH value, which can be measured via refractive index changes. In this part, the transmission spectra of the proposed MIM waveguide structure under different refractive index conditions are studied.
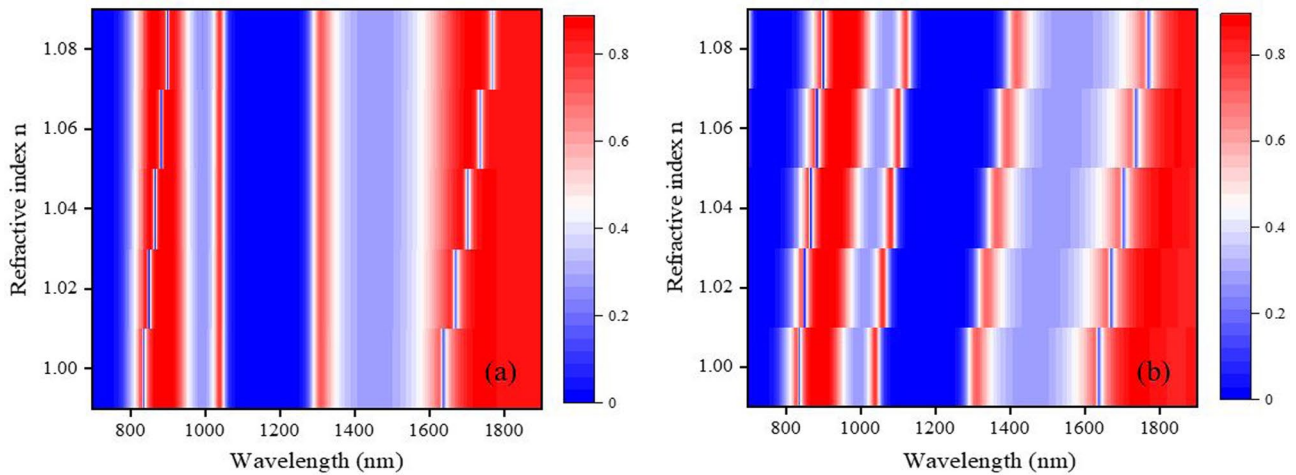
Figure 7a shows the sensitivity of the MIM waveguide structure as the variable refractive index media only fills the ring resonator. At this case, the results show that when the

refractive index of the medium increases from 1 to 1.08, both F1 and F4 modes have a significant red shift. F2 and F3 modes did not change with the refractive index of the medium in the ring resonator. Figure 7b shows the sensitivity of the entire MIM waveguide structure when the variable refractive index medium fills the entire MIM waveguide. The results show that when the refractive index of the medium increases from 1 to 1.08, F1, F2, F3, and F4 modes all have obvious red shifts. Comparing Fig. 7a, b, it can be proved once again that the ring resonator can control the F1 and F4 modes.

In sensing application region, the figure of merit (FOM) is an important factor to be considered to measure the sensing properties of the devices. The FOM is defined by the following equation [29] Eq. 8:

Fig. 6 Influence of parameters (**a**) r and (**b**) g on the transmission characteristics of the MIM waveguide structure

Fig. 7 Influence of environment refractive index on the transmission characteristics of the MIM waveguide structure. (**a**) The variable refractive index medium only fills the ring resonator. (**b**) The variable refractive index medium fills the entire MIM waveguide

$$\text{FOM} = \frac{S}{\text{FWHM}} = \frac{\delta\lambda/\delta n}{\text{FWHM}} \tag{8}$$

where $S = \delta\lambda/\delta n$ is the refractive index sensitivity which is calculated by resonance peak shift per index refractive of external medium, $\delta\lambda$ is the shift quantity of the resonance peak, δn is the change quantity of medium refractive, and FWHM is the full width at half maximum of the resonance line.

As shown in Table 1 and 2, the refractive index sensitivity and FOMs of the proposed MIM waveguide structure under different refractive index conditions are studied. In the first situation, when the media with different refractive indexes are only added to the ring resonator of the MIM waveguide structure, the refractive index sensitivity of F1 and F4 modes reached 800 nm/RIU and 1650 nm/RIU, respectively, and the FOM reached 88.9 and 117.8 in magnitude, respectively. In the second situation, when the same medium with different refractive index is added to the entire MIM waveguide structure, all four Fano resonances exhibit good refractive index sensitivity. Among F1, F2, F3, and F4, the refractive index sensitivity of F1 and F4 modes reached 800 nm/RIU and 1600 nm/RIU, which are basically similar to the first case. However, the FOM values are respective reached 100 and 123.2 in magnitude, which was slightly higher than the first situation that mainly due to the strengthening of the resonance of F1 and F4 at this time.

In addition, when the entire MIM waveguide structure is immersed in a different refractive index environment, F2 and F3 modes will also produce good refractive index sensitivity to environmental change, reaching 1000 nm/RIU and 1300 nm/RIU, respectively. However, due to the fact that the FWHM of F2 and F3 mode is relatively large, which directly causes their FOM values to be very small, which can only reach 23.8 and 18.1 in magnitude, respectively.

Eventually, under two different conditions, the refractive index sensitivity of the four Fano resonances in the MIM waveguide is much greater than that of sensors based on plasmonic nanostructures [30, 31]. In the meantime, for the superior sensitivity and FOM, the MIM waveguide structure is very sensitive to refractive index changes in the close vicinity of the waveguide structure surface, which fully demonstrate that the MIM waveguide structure with a smaller volume has potential applications in the near-infrared refractive index sensor and biosensors.

Table 1 Refractive index sensitivity and FOM of the MIM waveguide when the variable refractive index media only fills the ring resonator

Plasmon mode	F1	F4
RI sensitivity (nm/RIU)	800	1650
FOM	88.9	117.8

Table 2 Refractive index sensitivity and FOM of the MIM waveguide when the variable refractive index media fills the whole MIM waveguide

Plasmon mode	F1	F2	F3	F4
RI sensitivity (nm/RIU)	800	1000	1300	1600
FOM	100	23.8	18.1	123.2

Conclusion

In this paper, through the finite element method, the transmission spectrum characteristics of the MIM waveguide structure composed of two stubs resonator and a ring resonator are calculated. The results show that four Fano resonances can be realized in this MIM waveguide structure; furthermore, it can be confirmed that the Fano resonances F1 and F4 are adjusted by the ring resonator, and the Fano resonances F2 and F3 are controlled by the two stub resonators. Meanwhile, the two Fano resonances, F2 and F3, can form a stopband filter with a 149-nm stopband width. In addition, the MIM waveguide device has ideal sensitivity to changes in the refractive index of the surrounding environment, and can be used to identify materials with different refractive index characteristics. Therefore, the MIM waveguide structure we proposed can not only effectively excite and flexibly adjust multi-Fano resonances but also can be applied to optical devices that rely on Fano resonance, such as the stop-band filters and refractive index sensors devices.

Data Availability The data that support the plots within this paper can be available from the corresponding author upon reasonable request.

Code Availability There is no code in this paper.

Declarations

Conflict of Interest The authors declare no competing interests.

References

1. Barnes WL, Dereux A, Ebbesen TW (2003) Surface plasmon subwavelength optics. Nature 424:824–830
2. Kano H, Mizuguchi S, Kawata S (1998) Excitation of surface-plasmon polaritons by a focused laser beam. Josa B 15:1381–1386
3. Hooper IR, Sambles JR (2002) Dispersion of surface plasmon polaritons on short-pitch metal gratings. Phys Rev B 65:165432
4. Zhang T, Wang J, Liu Q, Zhou JZ, Dai J, Han X, Li JQ, Zhou Y, Xu K (2019) Efficient spectrum prediction and inverse design for plasmonic waveguide systems based on artificial neural networks. Photonics Res 7:368
5. Dickson RM, Lyon LA (2000) Unidirectional plasmon propagation in metallic nanowires. J Phys Chem B 104:6095–6098
6. Gramotnev DK, Pile DFP (2004) Single-mode subwavelength waveguide with channel plasmon-ploartons in triangular grooves on a metal surface. Appl Phys Lett 85:6323–6325
7. Nikolajsen T, Leosson K, Bozhevolnyi SI (2005) In-line extinction modulator based on long-range surface plasmon polaritons. Opt Commun 244:455–459
8. Han Z, Forsberg E, He S (2007) Surface plasmon Bragg gratings formed in metal-insulator-metal waveguides. IEEE Photonics Technol Lett 19:91–93
9. Nikolajsen T, Leosson K, Bozhevolnyi S (2004) Surface plasmon polariton based modulators and switches operating at telecom wavelengths. Appl Phys Lett 85:5833–5835
10. Lin XS, Huang XG (2009) Numerical modeling of a teeth-shaped nano-plasmonic waveguide filter. J Opt Soc Am B 26:1263–1268
11. Zhai X, Wang L, Wang LL, Li XF, Huang WQ, Wen SH, Fan DY (2013) Tuning bandgap of a double-tooth-shaped MIM waveguide filter by control widths of the teeth. J Opt 15:055008
12. Zhu JH, Q. Wang J, Shum P, (2011) A nanoplasmonic high-pass wavelength filter based on a metal-insulator-metal circuitous waveguide. IEEE Trans Nanotechnol 10:1357–1361
13. Zafar R, Salim M (2014) Wideband slow light achievement in MIM plasmonic waveguide by controlling Fano resonance. Infrared Phys Technol 67:25–29
14. Yang ZJ, Hao ZH, Lin HQ, W QQ, (2014) Plasmonic Fano resonances in metallic nanorod complexes. Nanoscale 6:4985–4997
15. Chen F, Yao DZ (2016) Realizing of plasmon Fano resonance with a metal nanowall moving along MIM waveguide. Opt Commun 369:72–78
16. Liu N, Langguth L, Weiss T, Kastel J, Fleischhauer M, Pfau T, Giessen H (2009) Plasmonic analogue of electromagnetically induced transparency at the Drude damping limit. Nat Mater 8:758–762
17. Liu N, Weiss T, Mesch M, Langguth L, Eigenthaler U, Hirscher M, Sonnichsen C, Giessen H (2010) Planar metamaterial analogue of electromagnetically induced transparency for plasmonic sensing. Nano Lett 10:1103–1107
18. Guo ZC, Wen KH, Hu QY, Lai WH, Fang YH (2018) Plasmonic multichannel refractive index sensor based on subwavelength tangent-ring metal–insulator–metal waveguide. Sensors 18:1348
19. Luk'Yanchuk B, Zheludev NI, Maier SA, Halas NJ, Nordlander P, Giessen H, Chong CT (2010) The Fano resonance in plasmonic nanostructures and metamaterials[J]. Nat Mater 9:707–715
20. Hu F, Yi H, Zhou Z (2011) Band-pass plasmonic slot filter with band selection and spectrally splitting capabilities. Opt Express 19:4848–4855
21. Kwon SH (2013) Deep subwavelength-scale metal–insulator–metal plasmonic disk cavities for refractive index sensors. IEEE Photonics J 5:4800107
22. Shi XL, Ma LJ, Zhang ZD, Tang Y, Zhang YJ, Han JQ, Sun YQ (2018) Dual Fano resonance control and refractive index sensors based on a plasmonic waveguide-coupled resonator system. Opt Commun 427:326–330
23. Zhang Y, Cui M (2019) Refractive index sensor based on the symmetric MIM waveguide structure. J Electron Mater 48:1005–1010
24. Li SL, Zhang YY, Song XK, Wang YL, Yu L (2016) Tunable triple Fano resonances based on multimode interference in coupled plasmonic resonator system. Opt Express 24:15351–15361
25. Zhang ZD, Wang RB, Zhang ZY, Tang J, Wang WD, Xue CY, Yan SB (2017) Electromagnetically induced transparency and refractive index sensing for a plasmonic waveguide with a stub coupled ring resonator. Plasmonics 12:1007–1013
26. Luo SW, Li B, Xiong DS, Zuo DL, Wang XB (2016) A high performance plasmonic sensor based on metal-insulator-metal waveguide coupled with a double-cavity structure. Plasmonics 12:223–227

27. Zhan ZD, Luo L, Xue CY, Zhang WD, Yan SB (2016) Fano resonance based on metal-insulator-metal waveguide-coupled double rectangular cavities for plasmonic nanosensors. Sensors 16:642

28. Zhu JH, Wang QJ, Shum P, Huang XJ (2011) A simple nanometeric plasmonic narrow-band filter structure based on metal–insulator–metal waveguide. IEEE Trans Nanotechnol 10:1371–1376

29. Maxime C, Brulé T, Stacey L, Wenli C, Mitradeep S, Benjamin C, Karen F, Wei P, Michael C, Jean-Francois M (2017) High figure of merit (FOM) of Bragg modes in Au-coated nanodisk arrays for plasmonic sensing. Small 13:1700908

30. Yan ZD, Wen XG, Gu P, Zhong H, Zhan P, Chen Z, Wang ZL (2017) Double Fano resonances in individual metallic nanostructure for high sensing sensitivity. Nanotechnology 28:475203

31. Zhang Y, Zhen YR, Neumann O, Day JK, Nordlander P, Halas NJ (2014) Coherent anti-Stokes Raman scattering with single-molecule sensitivity using a plasmonic Fano resonance. Nat Commun 5:4424

Publisher's Note Springer Nature remains neutral with regard to jurisdictional claims in published maps and institutional affiliations.